Network Alterations Precede Atrophy in Alzheimer's Disease Progression Subtypes

Bailey Berman[1,2], Sterre de Jonge[1], Wenjie Kang[1], Myrthe F. van Haaften[1], Meike W. Vernooij[1,3], Elisabeth J. Vinke[1,3], Esther E. Bron[1]

[1] Department of Radiology & Nuclear Medicine, Erasmus MC, Rotterdam, The Netherlands
[2] Department of Neurology, UMC Utrecht, Utrecht, The Netherlands
[3] Department of Epidemiology, Erasmus MC, Rotterdam, The Netherlands
s.dejonge@erasmusmc.nl

Abstract. Brain network disruption is often seen in preclinical Alzheimer's disease (AD) however, it is unclear whether network alterations precede atrophy in the disease progression sequence. To address this gap, this study incorporates graph-theory derived measures of network integrity and regional brain volumes derived from T1w brain MRI scans into SuStaIn, a disease progression and subtyping model. Using the data of 1,699 ADNI participants, two SuStaIn models were created: a baseline model containing only regional brain volumes, and a model including both volumetric and network measures. The volumetric-only model reproduced previously established atrophy-based subtypes, including a Typical, Cortical, and Subcortical group. In the combined model, the Typical group split into two subtypes which both showed early network changes, followed by atrophy in the amygdala and hippocampus. However, the Typical 1 subtype showed initial alterations in network integration and Typical 2 demonstrated early alterations in network segregation. This suggests that network alterations precede atrophy for participants with typical progression patterns, highlighting their potential as an early disease marker.

Keywords: Graph theory, Structural similarity networks, Disease progression modeling.

1 Introduction

Alzheimer's disease (AD) is characterized by a long preclinical window, with an estimated 10-20 years between disease onset and the emergence of cognitive symptoms when AD is typically diagnosed [1]. With the advent of anti-amyloid treatments, there is a pressing need for earlier diagnostics, as these are most effective before irreversible damage such as atrophy and cognitive decline has occurred. Identifying early disease markers, however, is complicated by heterogeneity in disease progression. Data-driven disease progression models (DPM) such as Subtype and Stage Inference (SuStaIn) have been developed to address this heterogeneity by identifying groups of patients with similar progression patterns while simultaneously considering disease stage [2]. When applied to imaging markers, SuStaIn has primarily incorporated regional brain volumes

to identify subtype-specific patterns of neurodegeneration. However, given that atrophy represents a process occurring late in disease progression [3], these models are limited in their ability to identify early disease markers that support timely diagnostics.

Incorporating measures of brain network integrity into DPMs may help capture earlier disease effects that precede atrophy or cognitive decline. PET studies have shown that early AD pathology tends to accumulate within connectivity networks [4,5], contributing to altered connectivity seen in preclinical AD [4,6–8]. Moreover, in autosomal dominant AD, reduced network integrity can be detected up to 12 years before symptom onset [9] and is predictive of future cognitive decline [10]. Thus, measures of network integrity may represent a link between early pathological processes and later cognitive decline, highlighting their potential for detecting and tracking disease progression.

Importantly, these network measures can be derived from routine T1w MRI scans by constructing structural similarity networks (SSN), which model connectivity as the statistical similarity of gray matter morphometry [11]. In AD, SSNs capture coordinated patterns of atrophy, as degenerating regions show similar gray matter properties [12]. However, given that patterns of atrophy overlap with known connectivity networks [13] and morphometrically similar regions tend to be structurally or functionally connected [12], these patterns remain interpretable in terms of connectivity, and offer a practical way to assess networks from the same MRI scan used to assess volumetry.

Yet, no studies have incorporated these network measures alongside volumetrics into disease progression and subtyping models. Consequently, it remains unclear whether network alterations precede regional atrophy in the inferred disease sequence and whether this ordering is consistent across subtypes. To address this gap, this study applies SuStaIn to regional brain volumes and graph theory-derived measures of network integrity computed from SSNs to assess the ordering of network and volumetric changes across AD subtypes. This model which combines network and volumetric measures will be compared to a baseline model which includes only brain volumes. It is expected that the atrophy-based subtypes from the volumetric-only model will be preserved in the combined model, and that network alterations will emerge at an earlier SuStaIn stage than volumetric changes for some subtypes.

2 Methods

2.1 Data

Population. Data was obtained from the Alzheimer's Disease Neuroimaging Initiative (ADNI) database (adni.loni.usc.edu). Participants from ADNI 1/2/GO who had available T1 scans acquired within 6 months of their baseline diagnostic visit were eligible for inclusion. For participants with multiple scans, the earliest scan was selected. The study population encompassed cognitively normal (CN) controls, as well as patients with mild cognitive impairment (MCI), and mild AD. A total of 1,721 participants were eligible for inclusion. However, 5 were excluded because the time between scan and diagnostic visit exceeded six months, and 17 additional participants were excluded because their network topology was too constrained to generate degree-preserving null models. The remaining 1,699 participants were included in the analysis.

MRI Acquisition and Processing. T1-weighted structural MRI data was acquired using 1.5T and 3T scanners. These scans were processed using FreeSurfer version 7.0 and segmented into 80 cortical and subcortical regions based on the Desikan-Killiany atlas. ComBat harmonization was performed across field strengths, including age and sex as covariates [14]. Images were further processed using FMRIB Software Library (FSL) version 5.0.6 to produce voxel-based morphometry (VBM) maps. Following a standard preprocessing pipeline, gray matter voxels were extracted from the FreeSurfer output and nonlinearly registered to the Montreal Neurological Institute (MNI) gray matter template at a 1x1x1 mm^3 resolution. Following modulation, the maps were smoothed with a 6-mm full width at half-maximum Gaussian kernel, as this has been shown to improve the reliability of graph theory metrics derived from VBM maps [15].

Cognitive Data. Various neuropsychological tests were used to assess cognitive profiles across subtypes, including the Boston Naming Test, Animal Fluency, Rey Auditory Verbal Learning Test (RAVLT) delayed recall, Logical Memory Test immediate recall, and Trail Making Test parts A and B. Only participants with cognitive data acquired within 6 months of the diagnostic visit and MRI scan were included. All cognitive tests were normalized with respect to the CN group and adjusted for age, sex, and years of education using linear regression.

2.2 Structural Similarity Networks

Following the approach outlined by Kong et al. (2015), the SSNs were constructed by modeling connectivity as the statistical similarity of gray matter distributions. This method was chosen because it retains spatial information about cortical thickness and folding structure, which is associated with white matter connectivity and vulnerability in dementia [16,17]. As such, it may yield a more biologically grounded connectivity map compared to other SSN approaches that rely on a single morphometric feature.

To construct the SSNs, the VBM maps were first parcellated into 90 regions based on the automated anatomical labeling (AAL) atlas. These regions defined the nodes of the network. Then, gray matter values were extracted for each node, and a probability density function was estimated using Kernel Density Estimation (KDE) (SciPy package, v1.16.3), with bandwidths chosen automatically using Scott's rule [18]. Next, similarity of gray matter distributions was calculated for each pair of regions using the symmetric Kullback-Leibler divergence formula converted into a similarity metric. The resulting Kullback-Leibler similarity (KLS) values represented the edges, or connections between nodes. These KLS values used to generate a 90x90 connectivity matrix for each individual subject, where high similarity is a proxy for connectivity.

Following matrix construction, spurious connections were removed by converting the matrices into binary, adjacency matrices using sparsity thresholding. Matrices were binarized across a range of sparsity levels (5-30% in steps of 2%). However, only densities ranging from 15-30% were used for graph theory calculations because at lower densities the largest connected component contained <80% of nodes in >10% of participants [19]. Graph theory metrics, including local efficiency, global efficiency, and

small-worldness were calculated at each sparsity level using the Python package NetworkX (v3.6.1) [20]. All metrics were normalized against 100 random networks generated via Maslov and Sneppen rewiring, and the normalized metrics were averaged across sparsity levels to produce a single value per metric per subject.

2.3 SuStaIn

This study implemented the z-score version of SuStaIn, which models disease progression as the linear accumulation of biomarkers from one z-score to the next. The z-score SuStaIn algorithm identifies groups of subjects (subtypes) with a shared sequence of z-score events, and the position of a subject in the sequence determines their stage.

Two SuStaIn models were specified: Model 1 included 13 brain volumes, covering the frontal, temporal, parietal, and occipital lobes, as well as the cingulate, insula, nucleus accumbens, amygdala, caudate, hippocampus, pallidum, putamen, and thalamus. These regions were selected to reproduce previously established ADNI atrophy-based subtypes [2]. Model 2 contained all volumes from Model 1, plus graph theory measures of small-worldness, local efficiency, and global efficiency. These metrics were selected as they each assess unique aspects of network topology: small-worldness measures the balance between integration and segregation, as assessed by path length and clustering respectively; local efficiency was selected as an alternative measure of segregation, and global efficiency was included as a measure of integration. Additionally, local and global efficiency were selected because they can be computed on disconnected graphs.

All biomarkers were normalized relative to the CN group using regression-based norming and corrected for age, sex and total intracranial volume for volumetric features. Additionally, volumetric biomarkers were multiplied by -1 to increase with disease progression. For each biomarker, the integer nearest the 99th percentile determined the maximum z-score, and each preceding integer was used as a z-score event, with the first event starting at a z-score of 1. Lastly, 10-fold cross-validation was performed separately for Models 1 and 2 to determine the optimal number of subtypes. The model with the lowest cross-validation information criterion (CVIC) and highest log likelihood was selected.

2.4 Statistical Analysis

ANOVA was used to assess differences in demographics and biomarker profiles across subtypes. However, as group differences may be confounded by different stage distributions per subtype, all metrics were adjusted for disease stage using linear regression. Tukey HSD post-hoc test was used to determine which groups showed statistically significant differences across these stage-adjusted metrics. All analyses were performed in Python v3.11 and the threshold for statistical significance was set at $p < 0.05$.

3 Results

3.1 Model 1

In line with past findings, Model 1 identified 3 atrophy-based subtypes: a Typical group (N = 580) with atrophy beginning in the amygdala and hippocampus; a Cortical subtype (N = 283) with early volume loss in the frontal, temporal, and parietal lobes; and a Subcortical subtype (N = 191) with atrophy beginning in the pallidum, putamen, and caudate. Participants whose biomarkers did not differ significantly from healthy controls, and could not be reliably subtyped, were assigned to the Stage 0 group (N = 645).

Table 1. Descriptives statistics for the full sample and subtypes from Model 1 (including volumetric and network measures). Continuous variables are presented as the mean (standard deviation) and categorical variables are presented as n (%). All biomarkers represent stage-adjusted z-scores, that increase with disease progression.

	Full sample	Stage 0	Typical	Cortical	Subcortical
N	1699	645	580	283	191
Sex (N males)	934 (55%)	338 (52%)	320 (55%)	162 (57%)	114 (60%)
Age	73.32 (7.16)	73.09 (6.96)	73.46 (6.83)	72.66 (8.03)	74.66 (7.37)
Education	15.82 (3.1)	16.15 (2.64)	15.38 (3.50)	15.65 (3.25)	16.29 (2.84)
CN	512 (30%)	316 (49%)	50 (9%)	83 (29%)	63 (33%)
MCI	851 (50%)	297 (46%)	319 (55%)	129 (46%)	106 (55%)
AD	336 (20%)	32 (5%)	211 (36%)	71 (25%)	22 (12%)
Amygdala	--	-0.26 (0.89)	1.22 (0.78)	0.23 (0.74)	-0.12 (0.73)
Hippocampus	--	-0.24 (0.81)	1.36 (0.75)	0.32 (0.8)	0.1 (0.72)
Global Efficiency	--	0.05 (0.97)	0.52 (0.85)	-0.31 (1.03)	0.07 (1.03)
Local Efficiency	--	0.05 (1.0)	0.16 (1.03)	0.11(1.18)	0.02 (1.03)
Small-worldness	--	0.06 (0.97)	0.28 (0.94)	0.07 (1.08)	0.07 (0.99)

3.2 Model 2

The combined SuStaIn model incorporating network measures revealed a 4-subtype structure (Δ CVIC > 8 over the 3-subtype solution), which included a Cortical (N = 407) and Subcortical (N = 139) subtype whose progression patterns mirrored those from Model 1. Additionally, two Typical subtypes were found, which showed distinct network profiles. The Typical 1 (N = 411) showed early changes in network integration, with global efficiency reaching a z-score of 1 in the first SuStaIn stage, followed by volume loss in the amygdala and hippocampus. The Typical 2 (N = 183) subtype showed initial changes in network segregation, with local efficiency and small-worldness reached z-scores of 2 in the first SuStaIn stages, followed by atrophy in the amygdala and hippocampus. Post-hoc analyses showed that the Typical 1 group had significantly increased global efficiency compared to all other subtypes ($p < 0.001$), more atrophy in the amygdala and hippocampus (all $p < 0.001$), and performed worse on memory (all $p < 0.01$) and language tests (all $p < 0.05$). Conversely, the Typical 2 group showed significantly increased network segregation ($p < 0.001$ for both local efficiency and clustering) and small-worldness ($p < 0.001$).

Table 2. Descriptives statistics for the subtypes from Model 2. Continuous variables are presented as the mean (standard deviation) and categorical variables are presented as n (%). All biomarkers represent stage-adjusted z-scores, that increase with disease progression.

	Stage 0	Typical 1	Cortical	Typical 2	Subcortical
N	559	411	407	183	139
Sex (N males)	300 (54%)	240 (58%)	221 (54%)	87 (48%)	86 (62%)
Age	73.29 (7.00)	73.80 (6.63)	72.79 (7.63)	72.57 (7.39)	74.57 (7.49)
Education	16.16 (2.68)	15.54 (2.94)	15.39 (3.84)	15.97 (2.78)	16.35 (2.88)
CN	287 (51%)	43 (10%)	89 (22%)	51 (28%)	42 (30%)
MCI	244 (44%)	230 (56%)	204 (50%)	91 (50%)	82 (59%)
AD	28 (5%)	138 (34%)	114 (28%)	41 (22%)	15 (11%)
Amygdala	-0.33 (0.86)	1.14 (0.74)	0.3 (0.68)	0.28 (0.94)	-0.29 (0.76)
Hippocampus	-0.28 (0.82)	1.26 (0.72)	0.39 (0.79)	0.32 (0.9)	-0.03 (0.76)
Global Efficiency	-0.02 (0.94)	0.84 (0.66)	-0.3 (0.98)	0.04 (0.95)	-0.08 (0.94)
Local Efficiency	-0.17 (0.87)	0.01 (0.8)	-0.18 (0.93)	1.72 (0.75)	-0.18 (0.95)
Small-worldness	-0.16 (0.86)	0.12 (0.75)	-0.08 (0.88)	1.64 (0.66)	-0.06 (0.9)

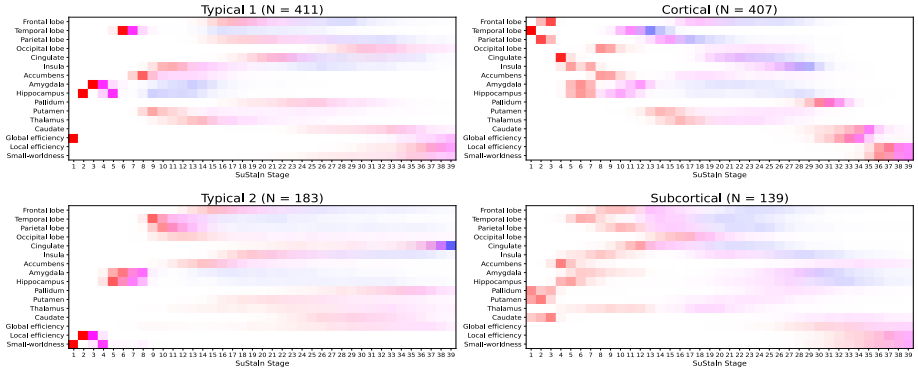

Fig. 1. Positional Variance Diagrams for subtypes from Model 2. The x-axis depicts disease stage and y-axis contains the biomarkers. The colors represent the z-score value for each biomarkers: red indicates a biomarker reaching a z-score of 1, magenta corresponds to z-score of 2, and blue corresponds to a z-score of 3. Higher z-scores correspond to more abnormal biomarkers. The opacity of the color reflects the certainty of a biomarker reaching a particular z-score at that stage.

3.3 Subtype Consistency Between Models

To assess consistency of subtype assignment across models, we computed the proportion of participants who were assigned the same subtype in Model 1 and Model 2. The Stage 0 and Cortical subtypes showed the highest consistency across models (83%), followed by the Subcortical subtype (70%). The Typical subtype from Model 1 showed 61% consistency. This is due to the fact that many subjects (N = 150) who were classified as Typical in Model 1 shifted to the Cortical subtype in Model 2. However, these participants were classified at late stages in both models, and subtype uncertainty is higher at late stages when most biomarkers reach abnormality. In addition, a portion of Stage 0 subjects from Model 1 were reclassified into the Typical 2 subtype in Model 2, suggesting that the inclusion of network measures in Model 2 enabled better classification of these participants within a subtype, as fewer participants were left unstaged.

4 Discussion

By incorporating network measures and regional brain volumes into SuStaIn, this study showed that network alterations precede atrophy in the inferred disease sequence for certain AD subtypes. The baseline, volumetric-only model replicated the established three-subtype structure, whereas the combined model revealed a four-subtype structure, including two Typical groups (Typical 1 and Typical 2) with distinct network profiles. The Typical 1 subtype showed initial alterations in network integration, whereas Typical 2 demonstrated early alterations in network segregation. These findings suggest that graph-theory derived measures of network integrity capture unique information about brain topology that helps distinguish AD subtypes, and that network alterations represent an early disease marker in these Typical groups.

4.1 Network Biomarkers Reveal Novel Subtype Structure

The Typical 1 subtype from the combined model closely resembled the Typical subtype from the volumetric-only model, with both groups showing significant atrophy in the amygdala and hippocampus, impaired memory, and increased segregation, as assessed by global efficiency. In contrast, the new Typical 2 subtype showed significantly increased integration, measured by local efficiency. This group was also younger, had relatively preserved cognition and mild global atrophy, suggesting it may represent a less advanced group of patients. The finding that the less impaired Typical 2 subtype is characterized by altered segregation and the more impaired Typical 1 group shows altered integration is in line with past literature showing that changes in segregation precede changes in integration. fMRI studies have reported increased segregation in preclinical AD due to amyloid induced hyperconnectivity within the Default Mode Network (DMN) [4,6]. However, as the disease progressed and amyloid accumulation plateaued, the DMN became disconnected. As a compensatory response, connectivity with other networks increased, leading to decreased segregation and a more integrated but less specialized connectome.

Thus, the Typical 1 and 2 groups may represent different positions along the same progression trajectory rather than truly distinct subtypes. The Typical 2 group may reflect an earlier stage, with increased segregation due to amyloid induced hyperconnectivity as seen in preclinical AD, whereas the Typical 1 group may represent a more advanced stage where increased global efficiency reflects a more integrated but randomly organized connectome. Therefore, the splitting of these two subtypes may reflect a limitation of the SuStaIn model, which assumes that biomarkers increase monotonically over time. However, this assumption that may not hold for measures of segregation, which have been shown to rise and fall as the disease progresses [6].

Regarding other network measures, the Typical 2 group also showed increased small-worldness which is calculated as the ratio between path length and clustering. However, path length measures showed large variability at lower densities (<20%) across both Typical groups, suggesting that the observed differences in small-worldness are likely driven by increased segregation (clustering) rather than increased integration. Additionally, it is notable that early network alterations were absent in the Cortical and

Subcortical groups. This could reflect the fact that early AD pathology preferentially targets the DMN, which is functionally and structurally connected to regions affected in the Typical subtypes, namely the amygdala and hippocampus. In contrast, the Cortical and Subcortical groups may not experience the same early, pathology-driven network disruption, which could explain why adding network measures did not alter their progression patterns.

4.2 Direction of Network Alterations

Another notable finding was that the Typical AD subtypes exhibited increased network segregation and integration relative to Stage 0 subjects. This may seem counter-intuitive; however, this finding is a consequence of defining connectivity as the statistical similarity of gray matter distributions: as regions atrophy, their gray matter distributions shift leftward in unison, which mathematically increases their similarity. Consequently, the graph metrics pick up on coordinated patterns of atrophy, as regions that show high similarity (connectivity) are atrophying in parallel. Therefore, increased segregation in the Typical groups may reflect spatially patterned atrophy due to a prion-like spread of amyloid within the DMN resulting in increased segregation [5]. Conversely, the Cortical and Subcortical subtypes may not show network alterations because their patterns of atrophy occur in a more diffuse or random way.

4.3 Limitations

There are several important limitations of this study. First, the measures of network segregation may violate SuStaIn's monotonicity assumption, which limits the ability to infer whether changes in network segregation precede changes in integration. Follow-up longitudinal analysis is necessary to validate the true ordering of network and volumetric changes. Second, this study used binarized graphs to compute graph theory metrics, which improves the interpretability of graphical analyses, but may provide a less accurate characterization of connectivity compared to weighted graphs [21]. Third, this study was performed in a presumed AD population, and similar network alterations occur in other neurodegenerative diseases. Thus, it remains unclear if these network changes are specific to early-stage AD.

4.4 Conclusion

By integrating individual-level network measures into SuStaIn, this study demonstrated that structural network alterations – which capture coordinated patterns of atrophy – emerged at an earlier stage than regional volumetric changes in Typical AD subtypes. The inclusion of network measures revealed heterogeneity within the Typical subtype, with one group showing early increased segregation and the other showing increased integration. This suggests that network measures capture early, disease-related changes that are not detectable using only volumetric biomarkers. In sum, these findings suggest that coordinated patterns of atrophy may be a more sensitive marker of early disease changes than volumetric measures in patients with Typical AD progression patterns.

References

1. Wu M, Thurston RC, Tudorascu DL, Karim HT, Mathis CA, Lopresti BJ, et al. Amyloid deposition is associated with different patterns of hippocampal connectivity in men versus women. Neurobiol Aging. 2019 Apr;76:141–50. doi:10.1016/j.neurobiolaging.2018.11.020
2. Young AL, Marinescu RV, Oxtoby NP, Bocchetta M, Yong K, Firth NC, et al. Uncovering the heterogeneity and temporal complexity of neurodegenerative diseases with Subtype and Stage Inference. Nat Commun. 2018 Oct 15;9(1):4273. doi:10.1038/s41467-018-05892-0
3. Bakhtiari A, Benedek K, Law I, Fagerlund B, Mortensen EL, Osler M, et al. Early cerebral amyloid-β accumulation and hypermetabolism are associated with subtle cognitive deficits before accelerated cerebral atrophy. GeroScience. 2024 Feb;46(1):769–82. doi:10.1007/s11357-023-01031-w PubMed PMID: 38102439; PubMed Central PMCID: PMC10828321.
4. Chang YT, Huang CW, Chang WN, Lee JJ, Chang CC. Altered Functional Network Affects Amyloid and Structural Covariance in Alzheimer's Disease. BioMed Res Int. 2018 Dec 2;2018:1–12. doi:10.1155/2018/8565620
5. Yu M, Sporns O, Saykin AJ. The human connectome in Alzheimer disease — relationship to biomarkers and genetics. Nat Rev Neurol. 2021 Sep;17(9):545–63. doi:10.1038/s41582-021-00529-1
6. Cha W, Chumin EJ, Yi D, Byun MS, Jung JH, Ahn H, et al. Amyloid-related default mode network hyperconnectivity and longitudinal decline in network distinctiveness in preclinical Alzheimer's disease. Alzheimers Dement. 2026 Feb;22(2):e71025. doi:10.1002/alz.71025
7. Mongay-Ochoa N, Gonzalez-Escamilla G, Fleischer V, Pareto D, Rovira À, Sastre-Garriga J, et al. Structural covariance analysis for neurodegenerative and neuroinflammatory brain disorders. Brain. 2025 Sep 3;148(9):3072–84. doi:10.1093/brain/awaf151
8. Xue C, Yuan B, Yue Y, Xu J, Wang S, Wu M, et al. Distinct Disruptive Patterns of Default Mode Subnetwork Connectivity Across the Spectrum of Preclinical Alzheimer's Disease. Front Aging Neurosci. 2019 Nov 13;11:307. doi:10.3389/fnagi.2019.00307
9. Vermunt L, Dicks E, Wang G, Dincer A, Flores S, Keefe SJ, et al. Single-subject grey matter network trajectories over the disease course of autosomal dominant Alzheimer's disease. Brain Commun. 2020 Jul 1;2(2):fcaa102. doi:10.1093/braincomms/fcaa102
10. Dicks E, Vermunt L, Van Der Flier WM, Barkhof F, Scheltens P, Tijms BM, et al. Grey matter network trajectories across the Alzheimer's disease continuum and relation to cognition. Brain Commun. 2020 Jul 1;2(2):fcaa177. doi:10.1093/braincomms/fcaa177
11. Sebenius I, Dorfschmidt L, Seidlitz J, Alexander-Bloch A, Morgan SE, Bullmore E. Structural MRI of brain similarity networks. Nat Rev Neurosci. 2025 Jan;26(1):42–59. doi:10.1038/s41583-024-00882-2
12. Alexander-Bloch A, Giedd JN, Bullmore E. Imaging structural co-variance between human brain regions. Nat Rev Neurosci. 2013 May;14(5):322–36. doi:10.1038/nrn3465
13. Seeley WW, Crawford RK, Zhou J, Miller BL, Greicius MD. Neurodegenerative Diseases Target Large-Scale Human Brain Networks. Neuron. 2009 Apr;62(1):42–52. doi:10.1016/j.neuron.2009.03.024
14. Fortin JP, Cullen N, Sheline YI, Taylor WD, Aselcioglu I, Cook PA, et al. Harmonization of cortical thickness measurements across scanners and sites. NeuroImage. 2018 Feb;167:104–20. doi:10.1016/j.neuroimage.2017.11.024
15. Wang H, Jin X, Zhang Y, Wang J. Single-subject morphological brain networks: connectivity mapping, topological characterization and test–retest reliability. Brain Behav. 2016 Apr;6(4):e00448. doi:10.1002/brb3.448

16. Sanabria-Diaz G, Melie-García L, Iturria-Medina Y, Alemán-Gómez Y, Hernández-González G, Valdés-Urrutia L, et al. Surface area and cortical thickness descriptors reveal different attributes of the structural human brain networks. NeuroImage. 2010 May 1;50(4):1497–510. doi:10.1016/j.neuroimage.2010.01.028 PubMed PMID: 20083210.
17. Pizzagalli F, Auzias G, Yang Q, Mathias SR, Faskowitz J, Boyd JD, et al. The reliability and heritability of cortical folds and their genetic correlations across hemispheres. Commun Biol. 2020 Sep 15;3(1):510. doi:10.1038/s42003-020-01163-1
18. Kong X zhen, Liu Z, Huang L, Wang X, Yang Z, Zhou G, et al. Mapping Individual Brain Networks Using Statistical Similarity in Regional Morphology from MRI. He H, editor. PLOS ONE. 2015 Nov 4;10(11):e0141840. doi:10.1371/journal.pone.0141840
19. Uehara T, Yamasaki T, Okamoto T, Koike T, Kan S, Miyauchi S, et al. Efficiency of a "Small-World" Brain Network Depends on Consciousness Level: A Resting-State fMRI Study. Cereb Cortex. 2014 Jun 1;24(6):1529–39. doi:10.1093/cercor/bht004
20. Hagberg A, Swart PJ, Schult DA. Exploring network structure, dynamics, and function using NetworkX. In. Los Alamos National Laboratory; 2007. doi:LA-UR-08-05495; LA-UR-08-5495
21. Rubinov M, Sporns O. Complex network measures of brain connectivity: Uses and interpretations. NeuroImage. 2010 Sep;52(3):1059–69. doi:10.1016/j.neuroimage.2009.10.003